

A multi-layer reduced model for flow in porous media with a fault and surrounding damage zones

Alessio Fumagalli Anna Scotti

March 5, 2019

Abstract

In this work we present a new conceptual model to describe fluid flow in a porous media system in presence of a large fault. Geological faults are often modeled simply as interfaces in the rock matrix, but they are complex structure where the high strain core is surrounded by the so called damage zones, characterized by the presence of smaller fractures which enhance the permeability of the medium. To obtain reliable simulation outcomes these damage zone, as well as the fault, have to be accurately described. The new model proposed in this work considers both these two regions as lower dimensional and embedded in the rock matrix. The model is presented, analyzed, and tested in several configurations to prove its robustness and ability to capture many important features, such as high contrast and heterogeneity of permeability.

1 Introduction

The accurate description and simulation of fluid flow in geological porous media are of paramount importance for several industrial applications, such as: CO₂ injection and sequestration, geothermal exploitation, oil migration and recovery, and prevention of groundwater contamination due to nuclear waste disposal, just to name a few. See [5, 28, 24]. Despite the relevance of the topic, a number of challenges are not yet fully solved, in particular related to the presence of faults and fractures in the domain of interest. Faults and fractures are the portion of the porous media where the rock has been broken due to geological movements of the upper crust. In this study we consider only large faults.

A tectonic fault is the result of a relative displacement of two parts of the upper crust happened over geological eras. This displacement is accommodate by a high strain region, the fault core, surrounded on both sides by a highly fractured region, the damage zone. These layer contain several fractures, on a much smaller scale than the fault, which may alter the local properties of the flow path. Faults have a thickness which is several order of magnitude smaller than any other characteristic sizes in the porous domain, however their physical properties may greatly differ from the porous media. Due to infilling processes and chemical reactions these objects may be partially or completely occluded, thus they can behave as preferential conduits or geological barriers for the fluid flow. The surrounding damage zone may or may not had experienced the same processes behaving similarly to, or differently from than the related fault. The development of accurate conceptual models is a key factor to be able to include these objects and their effect in a simulation code and obtain reliable outcomes and predictions. The aim of this work is to devise a new effective conceptual model to account for multiple thin regions in porous media.

One possibility to account for the presence of faults is to characterize this region with a different permeability, but its small thickness makes difficult or even unrealistic its inclusion in the grid representing the rock matrix. A common approach, introduced in [25, 40, 16, 20], is to consider faults as a lower dimensional objects and derive a new conceptual model to describe the flow and pressure behavior inside and across these objects. This approach has been successfully applied to different kind of physics, ranging from advection of a passive scalar, heat transport, multi-phase flow. An incomplete list of references is the following [31, 35, 23, 3, 32, 26, 12, 19, 18, 33, 22, 37, 30, 38, 13, 1, 10, 27, 8, 4, 39, 17, 7, 9, 34].

In this work we extend the previously introduced models to consider also the damage zone as a lower dimensional objects which are connected on one side to the rock matrix and, on the other side, to the fault. The aim is to be able to simulate different scenarios where the rock matrix, damage zone, and fault may have different permeability values without resorting to extreme mesh refinement to capture the thickness of the damage and core zones. Moreover this multilayer approach allows for different apertures and asymmetries across the fault, unlike the previous models.

The numerical discretization is based on the classical Raviart-Thomas-Nédélec approximation for the flux field and a constant piecewise representation of the pressure. The resulting scheme is locally mass conservative and is thus suitable for coupling with a transport problem. For clarity in the exposition, we consider only one single fault, since the case of intersecting faults requires additional model complexities.

For the implementation of the numerical examples, we have used the library PorePy [29], which is a simulation tool written in Python for fractured and deformable porous media. The numerical tests presented in this paper are available in the GitHub repository of the library. The main contribution of this work is the introduction of the multi-layers interface law, valid for any dimension. Even if we present an approximation and analysis based on the lowest order Raviart-Thomas-Nédélec, the implementation is agnostic with respect to the numerical scheme. It is indeed possible to use any other scheme present in the library, like two and multi point flux approximation or the mixed virtual element method.

The paper is organised as follow: in Section 2 both the equi and mixed-dimensional mathematical models are introduced and discussed. Section 3 deals with the weak formulation of the mixed-dimensional problem: functional spaces, weak problem, and its well posedness. In Section 4 we briefly describe the numerical scheme and how to handle the mixed-dimensional nature of the problem. Section 5 contains two numerical test to validate the proposed model. Finally, Section 6 is devoted to conclusions.

2 Mathematical problem

In this section we present the mathematical models considered to describe the pressure and Darcy velocity governed by the single-phase Darcy flow equations. In Subsection 2.1, we recall the classical formulation where the fault and the damage zone are considered equi-dimensional with respect to the rock matrix, i.e. are represented as two dimensional in a two dimensional porous matrix, and three dimensional in 3D. Their thickness is thus explicitly represented in the domain and captured by the computational grid. By considering a model reduction approach, Subsection 2.2 presents the new formulation where the fault and damage zone are now represented as lower-dimensional objects and new equations are introduced.

2.1 Equi-dimensional model

Let Ω denote the rock host matrix, μ denote the damage zone and γ the fault core. The interfaces M and Γ between these objects can be defined as $\overline{M} = \overline{\partial\Omega} \cap \overline{\mu}$ and $\overline{\Gamma} = \overline{\mu} \cap \overline{\gamma}$, respectively. We define $\partial\Omega_{\text{int}}$ as the part of the boundary of Ω which is in contact with M , and with $\partial\Omega$ the part of the boundary of Ω which is not in contact with M . We further subdivide $\partial\Omega$ into two parts, $\partial\Omega_p$ and $\partial\Omega_u$, such that $\overline{\partial\Omega} = \overline{\partial\Omega_p} \cup \overline{\partial\Omega_u}$ with $\partial\Omega_p \neq \emptyset$ and $\emptyset = \partial\Omega_p \cup \partial\Omega_u$. In $\partial\Omega_p$ we will impose natural boundary conditions, while in $\partial\Omega_u$ essential boundary conditions. In the same way, we define the boundary of the damage zone μ as $\partial\mu_{\text{int}}$ and $\partial\mu$, being the internal and external portion of the boundary of μ , respectively. The external part $\partial\mu$ can be divided into two parts $\partial\mu_p$ and $\partial\mu_u$ such that $\overline{\partial\mu} = \overline{\partial\mu_p} \cup \overline{\partial\mu_u}$ with $\partial\mu_p \neq \emptyset$ and $\emptyset = \partial\mu_p \cup \partial\mu_u$. In $\partial\mu_p$ we will impose natural boundary conditions, while in $\partial\mu_u$ essential boundary conditions. The same nomenclature is introduced for the fault γ . We define the unit normal \mathbf{n} , associated with $\partial\Omega_{\text{int}}$, which points from Ω to M . Similarly, we introduce the unit normal \mathbf{n}_μ , associated with $\partial\mu_{\text{int}}$, which points from μ to Γ . Finally, $\boldsymbol{\nu}$ is the external outward unit normal of the domain. See Figure 1 as an example.

We assume that the rock matrix Ω , damage zone μ , and fault γ have the same spatial dimension. The damage zone and fault are characterized by one of the dimension to be much (orders of magnitude) smaller than the others. We are interested in the mathematical description

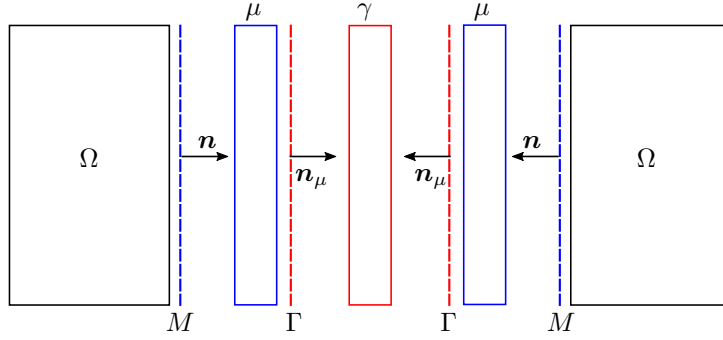


Figure 1: Equi-dimensional representation of the rock matrix Ω , damage zone μ , and fault γ .

of the Darcy velocity and pore pressure described by the Darcy problem. We indicate with p_Υ the pressure and with \mathbf{u}_Υ the Darcy velocity, on the portion (rock matrix, damage zone, or fault) Υ of the problem, being Υ equal to Ω , μ , and γ . The system of equations reads: find $(\mathbf{u}_\Upsilon, p_\Upsilon)$ such that

$$\begin{aligned}
 \sigma_\Upsilon^2 \mathbf{u}_\Upsilon + \nabla p_\Upsilon &= \mathbf{0} & \text{in } \Upsilon \\
 \nabla \cdot \mathbf{u}_\Upsilon + q_\Upsilon &= 0 & \\
 \text{tr } p_\Upsilon &= \overline{p_\Upsilon} & \text{on } \partial\Upsilon_p, \\
 \text{tr } \mathbf{u}_\Upsilon \cdot \boldsymbol{\nu} &= \overline{u_\Upsilon} & \text{on } \partial\Upsilon_u
 \end{aligned} \tag{1a}$$

The parameters are the inverse of the permeability σ_Υ^2 , the source or sink term q_Υ , and the boundary conditions on the pressure $\overline{p_\Upsilon}$ and velocity $\overline{u_\Upsilon}$. We make use of tr to indicate the trace operator. To couple the problem in the three domains, we consider the following transmission

conditions

$$\begin{aligned}
\operatorname{tr} \mathbf{u}_\Omega \cdot \mathbf{n} &= \operatorname{tr} \mathbf{u}_\mu \cdot \mathbf{n} && \text{on } M \\
\operatorname{tr} p_\Omega &= \operatorname{tr} p_\mu && \\
\operatorname{tr} \mathbf{u}_\mu \cdot \mathbf{n}_\mu &= \operatorname{tr} \mathbf{u}_\gamma \cdot \mathbf{n}_\mu && \text{on } \Gamma \\
\operatorname{tr} p_\mu &= \operatorname{tr} p_\gamma &&
\end{aligned} \tag{1b}$$

Even if not explicitly used in the previous set of equations, we indicate with ϵ_μ and ϵ_γ the thickness of the damage zone and fault, respectively. To summarize the equi-dimensional system of equations, we introduce the following problem.

Problem 1 (Equi-dimensional model problem). *Find $(\mathbf{u}_\Upsilon, p_\Upsilon)$ such that (1) is satisfied, for Υ equal to Ω , μ , and γ .*

2.2 Mixed-dimensional model

The geometrical reduction of the model approximates the thin regions, in our case the damage zone and the fault, by their center line (a lower dimensional object) and derives new equations and coupling conditions to describe the Darcy velocity and pressure field in the new setting. See Figure 2 as an example. In this work we follow the reduction procedure described in the literature in [2, 15, 31]. To keep the notation simple, we preserve the same notation for the rock matrix Ω , the damage zone μ and fault γ even if the domains are geometrically different from the equi-dimensional case: in particular Ω is extended up to the center line of the fault core, while the fault and the damage zone shrink and become overlapped lower dimensional interfaces.

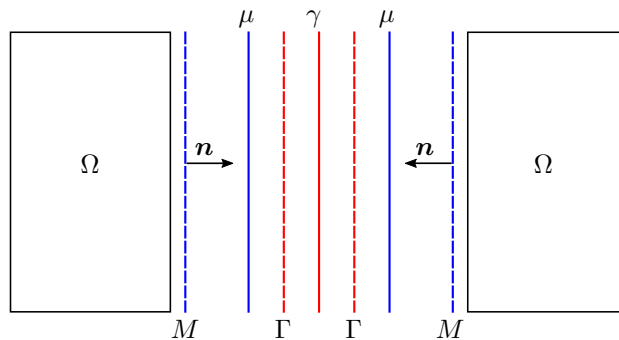


Figure 2: Mixed-dimensional representation of the rock matrix Ω , damage zone μ , and fault γ .

The mixed-dimensional problem describes the Darcy velocity and pressure field defined on the tangent space of each domain. At the interfaces, to couple the problems, we consider traces of the variables and the additional unknown u_Γ , which can be interpreted as a normal Darcy velocity from the damage zone μ to the fault γ . To simplify the notation, we introduce the pressure and Darcy velocity compounds p and \mathbf{u} , respectively, as

$$p = (p_\Omega, p_\mu, p_\gamma) \quad \text{and} \quad \mathbf{u} = (\mathbf{u}_\Omega, \mathbf{u}_\mu, \mathbf{u}_\gamma, u_\Gamma).$$

Note that \mathbf{u}_μ and \mathbf{u}_γ are fluxes in the lower dimensional layers and u_Γ is a scalar variable representing the normal flux exchanged by lower dimensional objects. Following the approaches

presented in [31, 40, 16, 20], we consider the Darcy model in each domain separately. First we consider the rock matrix,

$$\begin{aligned} \alpha_\Omega^2 \mathbf{u}_\Omega + \nabla p_\Omega &= \mathbf{0} & \text{in } \Omega \\ \nabla_\Omega \cdot \mathbf{u} + q_\Omega &= 0 \\ \text{tr } p_\Omega &= \overline{p}_\Omega & \text{on } \partial\Omega_p, \\ \text{tr } \mathbf{u}_\Omega \cdot \boldsymbol{\nu} &= \overline{u}_\Omega & \text{on } \partial\Omega_u, \end{aligned} \quad (2a)$$

where $\nabla_\Omega \cdot$ is the conservation operator (standard divergence) in the rock matrix. The parameters are α_Ω^2 which is the inverse of the rock matrix permeability, q_Ω which represents a scalar source or sink term, and \overline{p}_Ω and \overline{u}_Ω denoting the natural (pressure) and essential (flux) boundary data, respectively. In the damage zone μ the problem reads

$$\begin{aligned} \alpha_\mu^2 \mathbf{u}_\mu + \nabla p_\mu &= \mathbf{0} & \text{in } \mu \\ \nabla_\mu \cdot \mathbf{u} + q_\mu &= 0 \\ \text{tr } p_\mu &= \overline{p}_\mu & \text{on } \partial\mu_p, \\ \text{tr } \mathbf{u}_\mu \cdot \boldsymbol{\nu} &= \overline{u}_\mu & \text{on } \partial\mu_u, \end{aligned} \quad (2b)$$

where $\nabla_\mu \cdot$ is the conservation operator (mixed-dimensional divergence) which, as detailed below, accounts for the tangential divergence in μ and for the fluid exchanges between μ and γ , and μ and Ω . In (2b) α_μ^2 is the inverse of the effective matrix permeability in the damage zone, q_μ represents a scalar source or sink term, \overline{p}_μ and \overline{u}_μ are the natural and essential boundary data, respectively. In the fault core γ we have

$$\begin{aligned} \alpha_\gamma^2 \mathbf{u}_\gamma + \nabla p_\gamma &= \mathbf{0} & \text{in } \gamma \\ \nabla_\gamma \cdot \mathbf{u} + q_\gamma &= 0 \\ \text{tr } p_\gamma &= \overline{p}_\gamma & \text{on } \partial\gamma_p, \\ \text{tr } \mathbf{u}_\gamma \cdot \boldsymbol{\nu} &= \overline{u}_\gamma & \text{on } \partial\gamma_u, \end{aligned} \quad (2c)$$

where $\nabla_\gamma \cdot$ is the (inter-layer divergence) conservation operator accounting also for the exchange between the damage zone and the fault. In (2c) α_γ^2 is the inverse of the effective matrix permeability in the fault, q_γ represents a scalar source or sink term, \overline{p}_γ and \overline{u}_γ are the natural and essential boundary data, respectively. The conservation operators in each domain are defined as

$$\nabla_\Omega \cdot \mathbf{u} := \nabla \cdot \mathbf{u}_\Omega, \quad (2d)$$

$$\nabla_\mu \cdot \mathbf{u} := \nabla \cdot \mathbf{u}_\mu - \text{tr } \mathbf{u}_\Omega \cdot \mathbf{n} + u_\Gamma, \quad (2e)$$

$$\nabla_\gamma \cdot \mathbf{u} := \nabla \cdot \mathbf{u}_\gamma - u_\Gamma, \quad (2f)$$

where all the differential (divergence) operators are defined on the tangent space of the associated manifold. Moreover, these conservation operators account for the exchange terms between manifolds of, possibly, different dimensionality. To couple the problems we introduce the following interface laws which can be interpreted as projections of the Darcy law in the direction normal to the interfaces.

$$\begin{aligned} \alpha_M^2 \text{tr } \mathbf{u}_\Omega \cdot \mathbf{n} + p_\mu - \text{tr } p_\Omega &= 0 & \text{on } M \\ \alpha_\Gamma^2 u_\Gamma + p_\gamma - p_\mu &= 0 & \text{on } \Gamma. \end{aligned} \quad (2g)$$

In the previous equations the data are: α_M^2 which is the inverse of the effective normal matrix permeability between the rock matrix and the damage zone and α_Γ^2 which is the inverse of the effective normal matrix permeability between the damage zone and the fault.

Problem 2 (Mixed-dimensional model problem). *Find (\mathbf{u}, p) such that (2) is satisfied.*

Remark 1. *In the mixed-dimensional Problem 2 we have used directly the effective permeabilities, i.e. the permeabilities already scaled by the thickness of the related object. They can be related with the parameters of the equi-dimensional Problem 1 as follows*

$$\sigma_\Omega = \alpha_\Omega, \quad \sigma_\mu^2 = \alpha_M^2 \epsilon_\mu \mathbf{n} \otimes \mathbf{n} + \frac{\alpha_\mu^2}{\epsilon_\mu} (I - \mathbf{n} \otimes \mathbf{n}), \quad \sigma_\gamma^2 = \alpha_\Gamma^2 \epsilon_\gamma \mathbf{n}_\mu \otimes \mathbf{n}_\mu + \frac{\alpha_\gamma^2}{\epsilon_\gamma} (I - \mathbf{n}_\mu \otimes \mathbf{n}_\mu).$$

3 Weak problem

In this section we introduce the functional setting and the weak formulation of Problem 2. For simplicity, we consider null flux essential boundary conditions which, through a lifting technique, can be generalized. In the forthcoming parts we indicate with $\|\cdot\|_A$ the L^2 -norm on the set A and with $(\cdot, \cdot)_A$ the L^2 -scalar product on the set A .

3.1 Functional space setting

Since the previous problem couples unknowns in all the domains, it is natural to introduce a global functional space to respect this structure. The key motivation is related to the mixed-dimensional divergence operators, (2d) that are related to a space that generalise the classical (weighted) $H_{\nabla, \cdot}$ -space in this framework. For the vector fields, i.e. $\mathbf{u} = (\mathbf{u}_\Omega, \mathbf{u}_\mu, \mathbf{u}_\gamma, u_\Gamma)$, we introduce the following

$$\begin{aligned} V := \{ \mathbf{v} = (v_\Omega, v_\mu, v_\gamma, v_\Gamma) : \\ \alpha_\Omega v_\Omega \in L^2(\Omega) \wedge \alpha_M \operatorname{tr} v_\Omega \cdot \mathbf{n} \in L^2(M) \wedge \nabla_\Omega \cdot \mathbf{v} \in L^2(\Omega) \wedge \operatorname{tr} v_\Omega \cdot \boldsymbol{\nu} = 0 \text{ on } \partial\Omega_u, \\ \alpha_\mu v_\mu \in L^2(\mu) \wedge \nabla_\mu \cdot \mathbf{v} \in L^2(\mu) \wedge \operatorname{tr} v_\mu \cdot \boldsymbol{\nu} = 0 \text{ on } \partial\mu_u, \\ \alpha_\gamma v_\gamma \in L^2(\gamma) \wedge \nabla_\gamma \cdot \mathbf{v} \in L^2(\gamma) \wedge \operatorname{tr} v_\gamma \cdot \boldsymbol{\nu} = 0 \text{ on } \partial\gamma_u, \\ \alpha_\Gamma v_\Gamma \in L^2(\Gamma) \}, \end{aligned} \quad (3)$$

with the associated norm that make the space V complete, defined as

$$\begin{aligned} \|\mathbf{v}\|_V^2 := & \|\alpha_\Omega v_\Omega\|_\Omega^2 + \|\nabla_\Omega \cdot \mathbf{v}\|_\Omega^2 + \|\alpha_M \operatorname{tr} v_\Omega \cdot \mathbf{n}\|_M^2 + \|\alpha_\mu v_\mu\|_\mu^2 + \|\nabla_\mu \cdot \mathbf{v}\|_\mu^2 + \\ & \|\alpha_\gamma v_\gamma\|_\gamma^2 + \|\nabla_\gamma \cdot \mathbf{v}\|_\gamma^2 + \|\alpha_\Gamma v_\Gamma\|_\Gamma^2. \end{aligned}$$

We assume that exists $c_\Omega > 0$ such that $c_\Omega \leq \alpha_\Omega$ a.e., and $\alpha_\Omega \in L^\infty(\Omega)$. Similarly, we assume that there exists $c_M > 0$ such that $c_M \leq \alpha_M$ a.e., and $\alpha_M \in L^\infty(M)$. For the damage zone, we require that exists $c_\mu > 0$ such that $c_\mu \leq \alpha_\mu$ a.e., and also $\alpha_\mu \in L^\infty(\mu)$. Again, we assume that exists $c_\gamma > 0$ such that $c_\gamma \leq \alpha_\gamma$ a.e., and also $\alpha_\gamma \in L^\infty(\gamma)$. Finally, we require that exists $c_\Gamma > 0$ such that $c_\Gamma \leq \alpha_\Gamma$ a.e., and also $\alpha_\Gamma \in L^\infty(\Gamma)$. The extra regularity required for the trace of v_Ω on M is related to the interface conditions on M which can be seen as a Robin-type boundary conditions for a problem in mixed form. For more details see [36, 31].

The functional space for the pressure is defined again on the compound, namely

$$Q := \{ v = (v_\Omega, v_\mu, v_\gamma) : v_\Omega \in L^2(\Omega), v_\mu \in L^2(\mu), v_\gamma \in L^2(\gamma) \},$$

with associated norm that make the space Q complete, given by

$$\|v\|_Q^2 := \|v_\Omega\|_\Omega^2 + \|v_\mu\|_\mu^2 + \|v_\gamma\|_\gamma^2.$$

Remark 2 (Boundary conditions). *The conditions related to the boundaries in the definition of (3) have to be interpreted in a proper way. The first condition $\text{tr } \mathbf{v}_\Omega \cdot \boldsymbol{\nu} = 0$ on $\partial\Omega_u$ corresponds to*

$$\langle \text{tr } \mathbf{v}_\Omega \cdot \boldsymbol{\nu}, w \rangle_{\partial\Omega_u} = 0 \quad \text{for all } w \in H_{0,0}^{\frac{1}{2}}(\partial\Omega_u)$$

with $\langle \cdot, \cdot \rangle_A$ the duality pairing defined as $\langle \cdot, \cdot \rangle_A : H^{-\frac{1}{2}}(A) \times H_{0,0}^{\frac{1}{2}}(A) \rightarrow \mathbb{R}$, with A a generic set. From standard results we have $\text{tr } \mathbf{v}_\Omega \cdot \boldsymbol{\nu} \in H^{-\frac{1}{2}}(\partial\Omega_u)$. In a similar way, the condition $\text{tr } \mathbf{v}_\mu \cdot \boldsymbol{\nu} = 0$ on $\partial\mu_u$ means

$$\langle \text{tr } \mathbf{v}_\mu \cdot \boldsymbol{\nu}, w \rangle_{\partial\mu_u} = 0 \quad \text{for all } w \in H_{0,0}^{\frac{1}{2}}(\partial\mu_u).$$

In this case, we have $\text{tr } \mathbf{v}_\mu \cdot \boldsymbol{\nu} \in H^{-\frac{1}{2}}(\partial\mu_u)$. Finally, the condition $\text{tr } \mathbf{v}_\gamma \cdot \boldsymbol{\nu} = 0$ on $\partial\gamma_u$ is interpreted similarly as

$$\langle \text{tr } \mathbf{v}_\gamma \cdot \boldsymbol{\nu}, w \rangle_{\partial\gamma_u} = 0 \quad \text{for all } w \in H_{0,0}^{\frac{1}{2}}(\partial\gamma_u).$$

In this case we have $\text{tr } \mathbf{v}_\gamma \cdot \boldsymbol{\nu} \in H^{-\frac{1}{2}}(\partial\gamma_u)$.

Remark 3. *A more rigorous approach requires the introduction of interpolation operators between $\partial\Omega_{\text{int}}$ and M , as well as between μ and Γ and also between γ and Γ . However, to simplify the presentation we consider them implicit.*

3.2 Weak formulation

We propose now the weak formulation of the previous problem. Again, we respect the mixed-dimensional nature of Problem 2 by introducing bilinear forms that consider variables defined on different domains. We first introduce the weighted H_∇ -mass bilinear form, indicated by α and defined as $\alpha : V \times V \rightarrow \mathbb{R}$ such that

$$\begin{aligned} \alpha(\mathbf{u}, \mathbf{v}) := & (\alpha_\Omega \mathbf{u}_\Omega, \alpha_\Omega \mathbf{v}_\Omega)_\Omega + (\alpha_M \text{tr } \mathbf{u}_\Omega \cdot \mathbf{n}, \alpha_M \text{tr } \mathbf{v}_\Omega \cdot \mathbf{n})_M + (\alpha_\mu \mathbf{u}_\mu, \alpha_\mu \mathbf{v}_\mu)_\mu + \\ & (\alpha_\gamma \mathbf{u}_\gamma, \alpha_\gamma \mathbf{v}_\gamma)_\gamma + (\alpha_\Gamma u_\Gamma, \alpha_\Gamma v_\Gamma)_\Gamma. \end{aligned}$$

The bilinear form associated to the conservation statement is given by: $\beta : Q \times V \rightarrow \mathbb{R}$ such that

$$\begin{aligned} \beta(p, \mathbf{v}) := & -(p_\Omega, \nabla_\Omega \cdot \mathbf{v})_\Omega - (p_\mu, \nabla_\mu \cdot \mathbf{v})_\mu - (p_\gamma, \nabla_\gamma \cdot \mathbf{v})_\gamma \\ = & -(p_\Omega, \nabla \cdot \mathbf{v}_\Omega)_\Omega + (p_\mu, \text{tr } \mathbf{v}_\Omega \cdot \mathbf{n})_M - (p_\mu, \nabla \cdot \mathbf{v}_\mu)_\mu - (p_\gamma, \nabla \cdot \mathbf{v}_\gamma)_\gamma - \\ & (p_\mu, v_\Gamma)_\Gamma + (p_\gamma, v_\Gamma)_\Gamma. \end{aligned}$$

The functionals, which contain the boundary data and source terms, are defined as: $G : V \rightarrow \mathbb{R}$ and $F : Q \rightarrow \mathbb{R}$ such that

$$\begin{aligned} G(\mathbf{v}) := & -\langle \overline{p}_\Omega, \text{tr } \mathbf{v}_\Omega \cdot \boldsymbol{\nu} \rangle_{\partial\Omega_p} - \langle \overline{p}_\mu, \text{tr } \mathbf{v}_\mu \cdot \boldsymbol{\nu} \rangle_{\partial\mu_p} - \langle \overline{p}_\gamma, \text{tr } \mathbf{v}_\gamma \cdot \boldsymbol{\nu} \rangle_{\partial\gamma_p} \\ F(v) := & (q_\Omega, v_\Omega)_\Omega + (q_\mu, v_\mu)_\mu + (q_\gamma, v_\gamma)_\gamma. \end{aligned}$$

Where we assume that the pressure boundary data are such that $\overline{p}_\Omega \in H^{\frac{1}{2}}(\partial\Omega_p)$, $\overline{p}_\mu \in H^{\frac{1}{2}}(\partial\mu_p)$, and $\overline{p}_\gamma \in H^{\frac{1}{2}}(\partial\gamma_p)$. We require also that the source terms belong to $(q_\Omega, q_\mu, q_\gamma) \in Q$.

Problem 3 (Weak formulation). *The weak formulation of Problem 2 reads: find $(\mathbf{u}, p) \in V \times Q$ such that*

$$\begin{aligned} \alpha(\mathbf{u}, \mathbf{v}) + \beta(p, \mathbf{v}) &= G(\mathbf{v}) \quad \forall \mathbf{v} \in V \\ \beta(v, \mathbf{u}) &= F(v) \quad \forall v \in Q. \end{aligned}$$

3.3 Well posedness

In the proof of the well posedness of the problem, some parts are inspired by [18, 21].

Theorem 1. *Problem 3 is well posed.*

Proof. The bilinear forms and functionals in Problem 3 are linear, so we first prove their continuity. For simplicity, we assume that the portions of the boundary $\partial\Omega_u$, $\partial\mu_u$, and $\partial\gamma_u$ are empty. A lifting technique can be used in the general case. By using Cauchy-Schwarz and triangular inequalities we get

$$|\alpha(\mathbf{u}, \mathbf{v})| \leq \|\alpha_\Omega \mathbf{u}_\Omega\|_\Omega \|\alpha_\Omega \mathbf{v}_\Omega\|_\Omega + \|\alpha_M \operatorname{tr} \mathbf{u}_\Omega \cdot \mathbf{n}\|_M \|\alpha_M \operatorname{tr} \mathbf{v}_\Omega \cdot \mathbf{n}\|_M + \|\alpha_\mu \mathbf{u}_\mu\|_\mu \|\alpha_\mu \mathbf{v}_\mu\|_\mu + \|\alpha_\gamma \mathbf{u}_\gamma\|_\gamma \|\alpha_\gamma \mathbf{v}_\gamma\|_\gamma + \|\alpha_\Gamma u_\Gamma\|_\Gamma \|\alpha_\Gamma v_\Gamma\|_\Gamma \leq \|\mathbf{u}\|_V \|\mathbf{v}\|_V$$

as well as for the β bilinear form

$$|\beta(p, \mathbf{v})| \leq \|p_\Omega\|_\Omega \|\nabla_\Omega \cdot \mathbf{v}\|_\Omega + \|p_\mu\|_\mu \|\nabla_\mu \cdot \mathbf{v}\|_\mu + \|p_\gamma\|_\gamma \|\nabla_\gamma \cdot \mathbf{v}\|_\gamma \leq \|p\|_Q \|\mathbf{v}\|_V.$$

For the functionals, we consider in addition the trace inequality associated to the H_∇ -spaces. We obtain

$$\begin{aligned} |G(\mathbf{v})| &\leq \|\overline{p_\Omega}\|_{H^{\frac{1}{2}}(\partial\Omega_p)} \|\operatorname{tr} \mathbf{v}_\Omega \cdot \boldsymbol{\nu}\|_{H^{-\frac{1}{2}}(\partial\Omega_p)} + \|\overline{p_\mu}\|_{H^{\frac{1}{2}}(\partial\mu_p)} \|\operatorname{tr} \mathbf{v}_\mu \cdot \boldsymbol{\nu}\|_{H^{-\frac{1}{2}}(\partial\mu_p)} + \|\overline{p_\gamma}\|_{H^{\frac{1}{2}}(\partial\gamma_p)} \|\operatorname{tr} \mathbf{v}_\gamma \cdot \boldsymbol{\nu}\|_{H^{-\frac{1}{2}}(\partial\gamma_p)} \leq c_G \|\mathbf{v}\|_V \\ |F(v)| &\leq \|q_\Omega\|_\Omega \|v_\Omega\|_\Omega + \|q_\mu\|_\mu \|v_\mu\|_\mu + \|q_\gamma\|_\gamma \|v_\gamma\|_\gamma \leq c_F \|v\|_Q, \end{aligned}$$

with the constants

$$\begin{aligned} c_G &= \max \left\{ \|\overline{p_\Omega}\|_{H^{\frac{1}{2}}(\partial\Omega_p)}, \|\overline{p_\mu}\|_{H^{\frac{1}{2}}(\partial\mu_p)}, \|\overline{p_\gamma}\|_{H^{\frac{1}{2}}(\partial\gamma_p)} \right\}, \\ c_F &= \max \left\{ \|q_\Omega\|_\Omega, \|q_\mu\|_\mu, \|q_\gamma\|_\gamma \right\}. \end{aligned}$$

Now, we move on to proving the coercivity of α on the kernel of β . Considering a function $\mathbf{w} \in V$ such that $\beta(v, \mathbf{w}) = 0$ for all $v \in Q$, we have by a particular choice of v the following results

$$\begin{aligned} v = (v_\Omega, 0, 0) &\Rightarrow (v_\Omega, \nabla_\Omega \cdot \mathbf{w})_\Omega = 0 \quad \forall v_\Omega \in L^2(\Omega) &\Rightarrow \nabla_\Omega \cdot \mathbf{w} = 0 \text{ a.e. in } L^2(\Omega) \\ v = (0, v_\mu, 0) &\Rightarrow (v_\mu, \nabla_\mu \cdot \mathbf{w})_\mu = 0 \quad \forall v_\mu \in L^2(\mu) &\Rightarrow \nabla_\mu \cdot \mathbf{w} = 0 \text{ a.e. in } L^2(\mu) \\ v = (0, 0, v_\gamma) &\Rightarrow (v_\gamma, \nabla_\gamma \cdot \mathbf{w})_\gamma = 0 \quad \forall v_\gamma \in L^2(\gamma) &\Rightarrow \nabla_\gamma \cdot \mathbf{w} = 0 \text{ a.e. in } L^2(\gamma) \end{aligned}$$

thus the norm of \mathbf{w} simplifies to

$$\|\mathbf{w}\|_V^2 = \|\alpha_\Omega \mathbf{v}_\Omega\|_\Omega^2 + \|\alpha_M \operatorname{tr} \mathbf{v}_\Omega \cdot \mathbf{n}\|_M^2 + \|\alpha_\mu \mathbf{v}_\mu\|_\mu^2 + \|\alpha_\gamma \mathbf{v}_\gamma\|_\gamma^2 + \|\alpha_\Gamma v_\Gamma\|_\Gamma^2.$$

We can prove the coercivity of α on the kernel of β , by simply notice that $\alpha(\mathbf{w}, \mathbf{w}) = \|\mathbf{w}\|_V^2$.

To prove the inf-sup condition, given a function $v \in Q$, we introduce the following auxiliary problems

$$\begin{array}{lll} -\nabla \cdot \nabla \varphi_\Omega = v_\Omega & \text{in } \Omega & -\nabla \cdot \nabla \varphi_\mu = v_\mu + v_\gamma \quad \text{in } \mu \\ -\operatorname{tr} \nabla \varphi_\Omega \cdot \mathbf{n} = v_\mu & \text{on } M & \varphi_\mu = 0 \quad \text{on } \partial\mu_p \\ \operatorname{tr} \varphi_\Omega = 0 & \text{on } M & -\nabla \cdot \nabla \varphi_\gamma = -v_\mu \quad \text{in } \gamma \\ \operatorname{tr} \varphi_\Omega = 0 & \text{on } \partial\Omega_p & \varphi_\gamma = 0 \quad \text{on } \partial\gamma_p \end{array}$$

while for the intersection Γ we have $\varphi_\Gamma = v_\mu + v_\gamma$. By assuming that the domains are regular enough, from [14] an elliptic regularity result can be used giving

$$\begin{aligned}\varphi_\Omega &\in H_*^2(\Omega) \quad \text{with} \quad \|\varphi_\Omega\|_{H_*^2(\Omega)} \leq \|v_\Omega\|_\Omega + \|v_\mu\|_\mu, \\ \varphi_\mu &\in H^2(\mu) \quad \text{with} \quad \|\varphi_\mu\|_{H^2(\mu)} \leq \|v_\mu\|_\mu + \|v_\gamma\|_\gamma, \\ \varphi_\gamma &\in H^2(\gamma) \quad \text{with} \quad \|\varphi_\gamma\|_{H^2(\gamma)} \leq \|v_\mu\|_\mu.\end{aligned}$$

The space $H_*^2(\Omega)$ is the broken H^2 -space defined on each connected component of Ω (e.g. the left and right part in Figure 2), its norm is defined coherently. We clearly have $\|\varphi_\Gamma\|_\Gamma \leq \|v_\mu\|_\mu + \|v_\gamma\|_\gamma$. By considering the function $\mathbf{w} \in V$ such that

$$\mathbf{w} = (\mathbf{w}_\Omega, \mathbf{w}_\mu, \mathbf{w}_\gamma, w_\Gamma) = (\nabla\varphi_\Omega, \nabla\varphi_\mu, \nabla\varphi_\gamma, \varphi_\Gamma),$$

we obtain that $-\nabla \cdot \mathbf{w}_\Omega = v_\Omega$ and $\text{tr } \mathbf{w}_\Omega \cdot \mathbf{n} = v_\mu$. For \mathbf{w}_μ and \mathbf{w}_γ we get that $-\nabla \cdot \mathbf{w}_\mu = v_\mu + v_\gamma$ and $-\nabla \cdot \mathbf{w}_\gamma = -v_\mu$, respectively. Finally, we have $w_\Gamma = v_\gamma + v_\mu$. This gives the following expressions for the mixed-dimensional divergences $\nabla_\Omega \cdot \mathbf{w} = -v_\Omega$, $\nabla_\mu \cdot \mathbf{w} = -v_\mu$, and $\nabla_\gamma \cdot \mathbf{w} = -v_\gamma$. The V -norm of \mathbf{w} can be bound by the Q -norm of v , in fact

$$\|\mathbf{w}\|_V^2 = \|\nabla\varphi_\Omega\|_\Omega^2 + \|\nabla\varphi_\mu\|_\mu^2 + \|\nabla\varphi_\gamma\|_\gamma^2 + \|\varphi_\Gamma\|_\Gamma^2 + \|v_\Omega\|_\Omega^2 + 2\|v_\mu\|_\mu^2 + \|v_\gamma\|_\gamma^2 \leq \|v\|_Q^2.$$

Finally we obtain the boundedness of β from below with this choice of \mathbf{w} , namely

$$\beta(v, \mathbf{w}) = \|v_\Omega\|_\Omega^2 + \|v_\mu\|_\mu^2 + \|v_\gamma\|_\gamma^2 = \|v\|_Q^2 \geq \|v\|_Q \|\mathbf{w}\|_V.$$

Thus the inf-sup condition is fulfilled, and following [11] we conclude that Problem 3 is well posed. \square

4 Numerical discretization

To keep the mixed nature of Problem 3 in the numerical approximation, we consider the lowest order Raviart-Thomas-Nédélec \mathbb{RT}_0 finite element for the Darcy velocity and piecewise constant \mathbb{P}_0 for the pressure in the domains Ω , μ , and γ . The choice of the pair $\mathbb{RT}_0 - \mathbb{P}_0$ is also motivated by their local mass conservation property and consistency with the functional spaces considered in the weak formulation.

We introduce a family of simplicial meshes approximations of the domains Ω , μ , γ , Γ respectively, which will be indicated with the same symbol. By assuming a matching discretization of the meshes at the interfaces, the approximation of the functional spaces are defined as

$$\begin{aligned}V_h &:= \mathbb{RT}_0(\Omega) \times \mathbb{RT}_0(\mu) \times \mathbb{RT}_0(\gamma) \times \mathbb{P}_0(\Gamma) \subset V \\ Q_h &:= \mathbb{P}_0(\Omega) \times \mathbb{P}_0(\mu) \times \mathbb{P}_0(\gamma) \subset Q,\end{aligned}$$

we introduce a set of base functions for the discrete spaces, such that

$$\begin{aligned}\mathbb{RT}_0(\Omega) &= \text{span}_{i \in \text{dof } \mathbb{RT}_0(\Omega)} \{\zeta_{\Omega,i}\} \quad \text{and} \quad \mathbb{P}_0(\Omega) = \text{span}_{i \in \text{dof } \mathbb{P}_0(\Omega)} \{\xi_{\Omega,i}\} \\ \mathbb{RT}_0(\mu) &= \text{span}_{i \in \text{dof } \mathbb{RT}_0(\mu)} \{\zeta_{\mu,i}\} \quad \text{and} \quad \mathbb{P}_0(\mu) = \text{span}_{i \in \text{dof } \mathbb{P}_0(\mu)} \{\xi_{\mu,i}\} \\ \mathbb{RT}_0(\gamma) &= \text{span}_{i \in \text{dof } \mathbb{RT}_0(\gamma)} \{\zeta_{\gamma,i}\} \quad \text{and} \quad \mathbb{P}_0(\gamma) = \text{span}_{i \in \text{dof } \mathbb{P}_0(\gamma)} \{\xi_{\gamma,i}\} \\ \mathbb{P}_0(\Gamma) &= \text{span}_{i \in \text{dof } \mathbb{P}_0(\Gamma)} \{\zeta_{\Gamma,i}\}.\end{aligned}$$

We assume that quadrature is performed exactly. We indicate with h the global mesh size of the discretization.

4.1 Matrix formulation

Given the choice of the discrete spaces, we can recast the weak formulation of the problem in term of a block matrix system. We introduce the block matrices related to the mass matrices

$$\begin{aligned} [A_\Omega]_{i,j} &:= (\alpha_\Omega \zeta_{\Omega,i}, \alpha_\Omega \zeta_{\Omega,j})_\Omega + (\alpha_M \text{tr } \zeta_{\Omega,i} \cdot \mathbf{n}, \alpha_M \text{tr } \zeta_{\Omega,j} \cdot \mathbf{n})_M \\ [A_\mu]_{i,j} &:= (\alpha_\mu \zeta_{\mu,i}, \alpha_\mu \zeta_{\mu,j})_\mu \quad [A_\gamma]_{i,j} := (\alpha_\gamma \zeta_{\gamma,i}, \alpha_\gamma \zeta_{\gamma,j})_\gamma \quad [A_\Gamma]_{i,j} := (\alpha_\Gamma \zeta_{\Gamma,i}, \alpha_\Gamma \zeta_{\Gamma,j})_\Gamma, \end{aligned}$$

the matrices associated with the conservation statement in each domain are defined as

$$[B_\Omega]_{i,j} := -(\xi_{\Omega,j}, \nabla \cdot \zeta_{\Omega,i})_\Omega \quad [B_\mu]_{i,j} := -(\xi_{\mu,j}, \nabla \cdot \zeta_{\mu,i})_\mu \quad [B_\gamma]_{i,j} := -(\xi_{\gamma,j}, \nabla \cdot \zeta_{\gamma,i})_\gamma,$$

while between the domains the coupling conditions are associated with the matrices

$$[G_\Omega]_{i,j} := -(\xi_{\mu,j}, \text{tr } \zeta_{\Omega,i} \cdot \mathbf{n})_M \quad [G_\mu]_{i,j} := -(\xi_{\mu,i}, \zeta_{\gamma,j})_\Gamma \quad [G_\gamma]_{i,j} := (\xi_{\gamma,i}, \zeta_{\gamma,j})_\Gamma.$$

We indicate with \mathbf{u} and \mathbf{p} the values of degrees of freedom associated with the Darcy velocity and pressure. We make use of a similar notation to indicate the source and boundary terms. The linear system associated with Problem 3 is

$$\begin{bmatrix} A_\Omega & B_\Omega & & & & & & & & & G_\Omega \\ B_\Omega^\top & & & & & & & & & & & \\ & & A_\mu & B_\mu & & & & & & & & \\ G_\Omega^\top & & B_\mu^\top & & & & & & & & G_\mu \\ & & & & A_\gamma & B_\gamma & & & & & & \\ & & & & B_\gamma^\top & & & & & & G_\gamma \\ & & & & & & G_\mu^\top & & & & & \\ & & & & G_\mu^\top & & & G_\gamma^\top & & & A_\Gamma \\ & & & & & & & & & & & \\ & & & & & & & & & & & \end{bmatrix} \begin{bmatrix} \mathbf{u}_\Omega \\ \mathbf{p}_\Omega \\ \mathbf{u}_\mu \\ \mathbf{p}_\mu \\ \mathbf{u}_\gamma \\ \mathbf{p}_\gamma \\ \mathbf{u}_\Gamma \end{bmatrix} = \begin{bmatrix} \mathbf{g}_\Omega \\ \mathbf{f}_\Omega \\ \mathbf{g}_\mu \\ \mathbf{f}_\mu \\ \mathbf{g}_\gamma \\ \mathbf{f}_\gamma \end{bmatrix}. \quad (4)$$

where we have avoided explicitly writing empty matrices. Since the bilinear forms associated to the matrices A_Ω , A_μ , A_γ , A_Γ are symmetric then also these matrices are symmetric, resulting in a symmetric global system with a saddle-point structure. We can introduce the following problem.

Problem 4 (Matrix formulation). *The matrix formulation of Problem 3 is: find (\mathbf{u}, \mathbf{p}) such that (4) is satisfied.*

To recast the previous system in terms of the pressures alone, we introduce the matrices

$$\begin{aligned} S_\Omega &:= B_\Omega^\top A_\Omega^{-1} B_\Omega \quad S_\mu := B_\mu^\top A_\mu^{-1} B_\mu + G_\Omega^\top A_\Omega^{-1} G_\Omega + G_\mu A_\Gamma^{-1} G_\mu^\top \\ S_\gamma &:= B_\gamma^\top A_\gamma^{-1} B_\gamma + G_\gamma A_\Gamma^{-1} G_\gamma^\top \quad C_\Omega := B_\Omega^\top A_\Omega^{-1} G_\Omega \quad C_\mu := G_\mu^\top A_\Gamma^{-1} G_\mu^\top, \end{aligned}$$

where the matrices A_Ω , A_μ , A_γ , and A_Γ are invertible since they are a Raviart-Thomas-Nédélec approximation of the H_∇ -mass bilinear forms and $\partial\Omega_p \neq \emptyset$, $\partial\mu_p \neq \emptyset$, and $\partial\gamma_p \neq \emptyset$, while A_Γ is invertible by construction. The previous matrices are thus well defined and S_Ω , S_μ , S_γ are also symmetric and positive definite. We introduce the vectors

$$\begin{aligned} \mathbf{r}_\Omega &:= -\mathbf{f}_\Omega + B_\Omega^\top A_\Omega^{-1} \mathbf{g}_\Omega \quad \mathbf{r}_\mu := -\mathbf{f}_\mu + B_\mu^\top A_\mu^{-1} \mathbf{g}_\mu + G_\Omega^\top A_\Omega^{-1} \mathbf{g}_\Omega \\ \mathbf{r}_\gamma &:= -\mathbf{f}_\gamma + B_\gamma^\top A_\gamma^{-1} \mathbf{g}_\gamma, \end{aligned}$$

which are again well defined. The system in terms of pressure can be written as

$$\begin{bmatrix} S_\Omega & C_\Omega & & \\ C_\Omega^\top & S_\mu & C_\mu & \\ & C_\mu^\top & S_\gamma & \end{bmatrix} \begin{bmatrix} \mathbf{p}_\Omega \\ \mathbf{p}_\mu \\ \mathbf{p}_\gamma \end{bmatrix} = \begin{bmatrix} \mathbf{r}_\Omega \\ \mathbf{r}_\mu \\ \mathbf{r}_\gamma \end{bmatrix}. \quad (5)$$

Problem 5 (Pressure matrix formulation). *The pressure matrix formulation of Problem 3 is: find \mathbf{p} such that (5) is satisfied.*

To numerically solve the problem, it is possible to use the equivalent formulations of Problem 4 or Problem 5.

5 Numerical examples

In this part we present some numerical examples to show different aspects of the mathematical model introduced previously. In particular, we focus on its behavior in the presence of high contrasts in permeability among the rock matrix, damage zone and fault. We present also the model error, i.e. the error introduced by the geometrical reduction of the three layers and discuss the obtained results. Finally, we show the applicability in a three-dimensional domain.

All the test cases are implemented in the library PorePy [29]. The current implementation in the code considers a mortar variable on each interface and it is thus capable to handle non-matching discretization. Also, the code is agnostic with respect to the numerical scheme adopted in each domain. However, to keep the presentation simple and coherent with the previous sections, we will consider matching grids and Raviart-Thomas-Nédélec finite element of the lowest order for the numerical approximation.

5.1 Example 1

This first set of numerical tests is divided in two parts. In the first we present the effect of permeability heterogeneity in the fault and damage zone on the solution. This test is inspired by the examples presented in [31, 19]. We study the case of high permeability, low permeability, and a mixed case. The aim is to present the potentialities of the introduced model in the Sub-subsection 5.1.1. In the second part, Sub-subsection 5.1.2, the model error is studied comparing the mixed-dimensional solution with the equi-dimensional one where a full Darcy problem is solved on a computational grid refined enough to resolve the aperture of both the damage zone and the fault.

In all the cases we consider a fixed geometry and boundary conditions on the rock matrix. The rock matrix occupies the domain $\Omega = (0, 1) \times (0, 1) \cup (1, 2) \times (0, 1)$, while the damage zone and fault are identified as $\mu = \{1\} \times (0, 1)$ and $\gamma = \{1\} \times (0, 1)$, respectively. We set $\alpha_\Omega = 1$ and pressure boundary condition on the left and right of Ω , with values 0 and 1, respectively. On the remaining portions of the boundary we impose zero flux. The computational domain is represented in Figure 2. The grid is composed of $\sim 8.5k$ triangles for Ω , 80 segments for μ , 40 segments for γ , and 40 segments for Γ .

We consider three different sub-cases, depending on the value of α in the damage zone and fault. In all the cases, we set $\epsilon = 10^{-2}$. In the *case (i)* we have $\alpha_\mu^2 = 10^2\epsilon$ and $\alpha_M^2 = 10^2/\epsilon$ for the damage zone, and $\alpha_\gamma^2 = 10^2\epsilon$ and $\alpha_\Gamma^2 = 10^2/\epsilon$ for the fault. For the *case (ii)*, the parameters are chosen as $\alpha_\mu^2 = k\epsilon$ and $\alpha_M^2 = k/\epsilon$ for the damage zone, and $\alpha_\gamma^2 = k\epsilon$ and $\alpha_\Gamma^2 = k/\epsilon$ for the fault, where k is given by

$$k(y) = \begin{cases} 1 & \text{if } y < 0.25 \text{ or } y > 0.75 \\ 2 \cdot 10^{-3} & \text{if } 0.25 \leq y \leq 0.75. \end{cases}$$

Finally, in *case (iii)* we impose the values of $\alpha_\gamma^2 = k\epsilon$ and $\alpha_\Gamma^2 = k/\epsilon$ for the fault. The damage zone is divided into its left and right parts, on the former we have $\alpha_\mu^2 = k\epsilon$ and $\alpha_M^2 = k/\epsilon$ while on the latter $\alpha_\mu^2 = 10^2\epsilon$ and $\alpha_M^2 = 10^2/\epsilon$. In *case (i)* the lower dimensional objects are highly

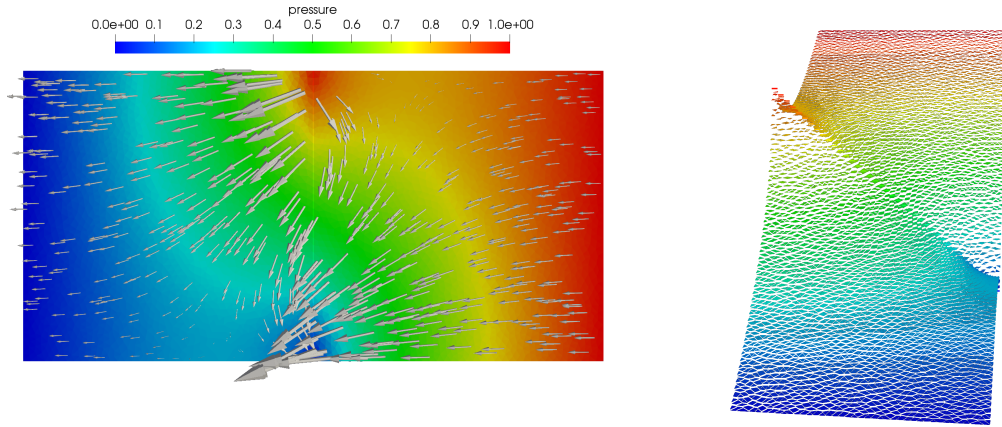


Figure 3: Graphical representation of the solution of *case (i)*. On the left the pressure field and the Darcy velocity, the latter shown only for few cells. On the right the pressure field warped and rotated.

conductive, in *case (ii)* are heterogeneous in space and less conductive in the central part, and in *case (iii)* the damage zone is heterogeneous in space and asymmetric.

In *case (i)* we impose unitary pressure at damage zone and fault tips $y = 1$, while zero pressure on the other side. For *case (ii)* and *case (iii)* zero flux is imposed on the boundary of the damage zone and fault.

5.1.1 Permeability contrast

In this first section, we present the numerical results obtained from the reduced model in the three different cases. In Figure 3 the results from *case (i)* are shown. Due to the high value of α_μ , α_M , α_γ , and α_Γ the pressure profile is smooth (continuous) across μ and γ . The impact of these lower dimensional objects on the flow is still quite remarkable, due to the type of boundary conditions and the permeability contrast.

The solution for the *case (ii)* is given in Figure 4. The impact of the low value of the permeabilities in the central parts of μ and γ is evident. We have a pressure jump between the rock matrix and the damage zone, and between the damage zone and the fault. The pressure in the latter is constant due to the symmetry of the problem. The flow tends to focus around these less permeable regions.

Figure 5 shows the results from the *case (iii)*. In this test a side of μ has a portion with low α_μ and α_M , while on the other side these coefficients have high values. The pressure solution exhibit thus a jump between the rock matrix and the first side of μ , and with the latter and the fault. However, on the other side the solution behaves similarly to *case (i)* and we obtain a smooth (continuous) profile among the fault and the second part of μ and the fault. The Darcy velocity tends to avoid the low permeable part of μ , but not the high permeable one.

The test cases above demonstrate the capability of the model to handle different combinations of the model parameters. The obtained solutions are physically sound and show the capability and potentiality of the model.

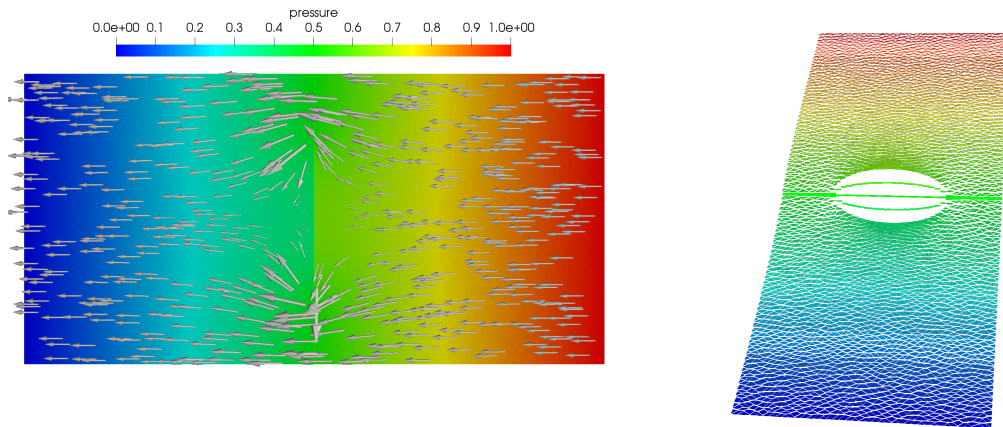


Figure 4: Graphical representation of the solution of *case (ii)*. On the left the pressure field and the Darcy velocity, the latter shown only for few cells. On the right the pressure field warped and rotated.

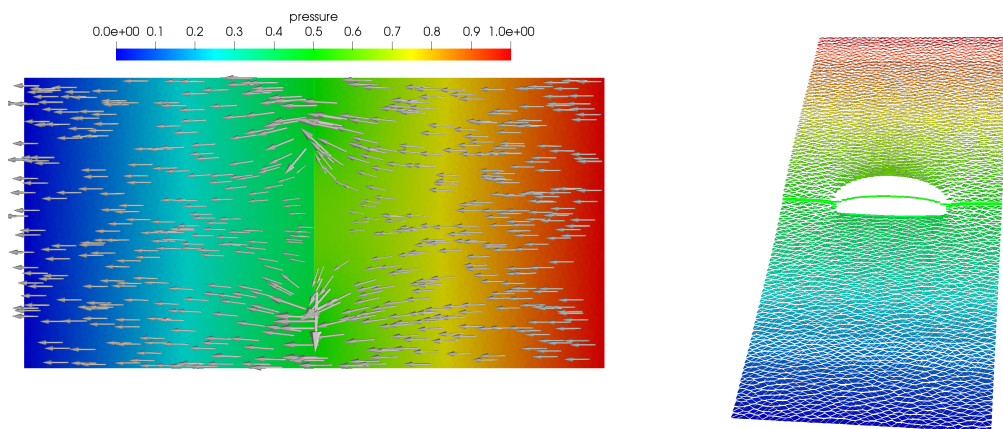


Figure 5: Graphical representation of the solution of *case (iii)*. On the left the pressure field and the Darcy velocity, the latter shown only for few cells. On the right the pressure field warped and rotated.

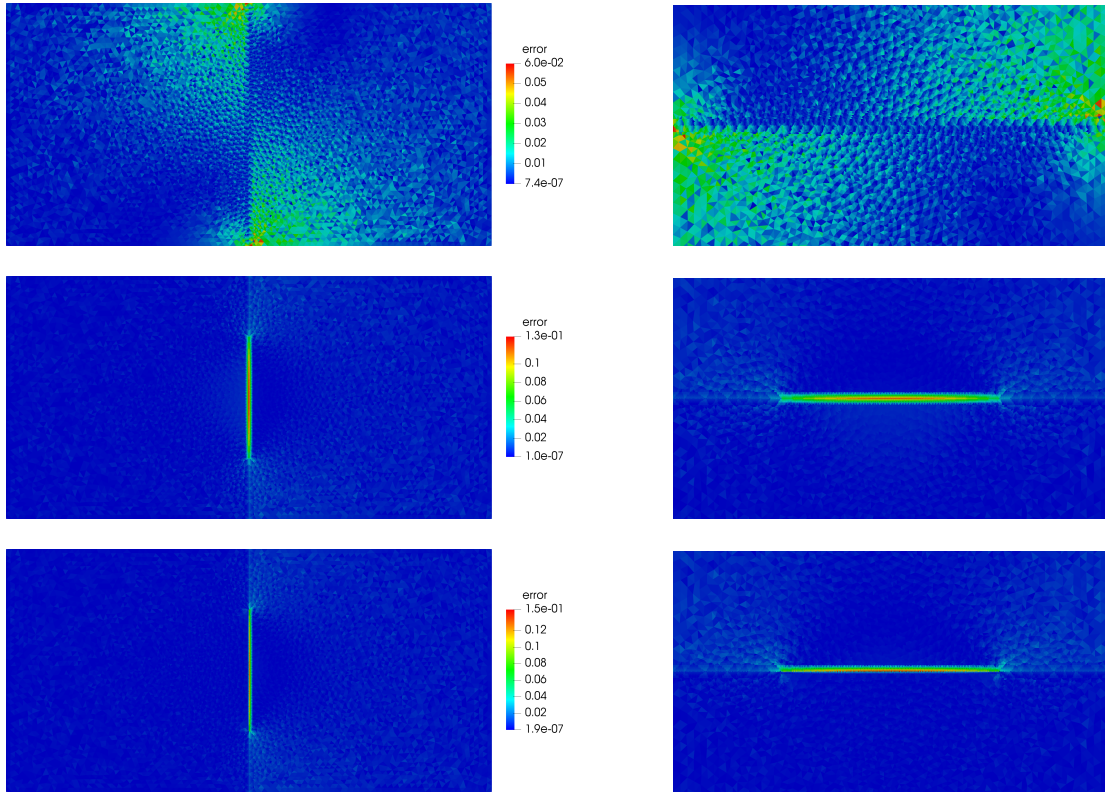


Figure 6: Graphical representation of the solution of *case (iii)*. On the left the pressure field and the Darcy velocity, the latter shown only for few cells. On the right the pressure field warped and rotated. The pressure is scaled in $[0, 1]$, from red to blue.

5.1.2 Model error

In this section we discuss the error associated with the geometrical reduction of the fault and damage zone, which are modeled as $n - 1$ dimensional interfaces even if, physically, they are n dimensional regions as Ω . To estimate this error we will compare the solutions provided by the mixed-dimensional model with the numerical solution of a traditional full Darcy problem set on a domain with heterogeneous permeabilities, discretized with a grid that is able to resolve the actual aperture of the layers. The equi-dimensional solution is computed with the same pair of mixed finite elements as the mixed-dimensional one. Let p_{equi}^η be the numerical solution of the equi-dimensional problem on a grid \mathcal{T}_η of size η . Let $I^\eta(p_\Omega^h)$ be the interpolation of p_Ω^h on \mathcal{T}_η ; in Figure 6 we show the difference $I^\eta(p_\Omega^h) - p_{\text{equi}}^\eta$ for the three cases presented in the previous section.

We can observe that, as expected, for the second and third cases the difference is mostly focused in the fault and surrounding layers: there indeed the equi-dimensional solution exhibits strong gradients which are replaced by jumps in the mixed-dimensional approximation due to the shrinking of the layers into interfaces. It can also be observed the asymmetry in the model error of the third case, reflecting the different permeabilities of the two layers of the damage zone. In the first case however, where the fault is conductive, pressure is continuous everywhere and the largest values of the error are due to the strong gradients close to the fault which are

ϵ	case (i)	case (ii)	case (iii)
10^{-2}	1.12812e-2	9.72846e-3	8.93785e-3
$5 \cdot 10^{-3}$	7.29157e-3	6.83495e-3	6.36322e-3
$2.5 \cdot 10^{-3}$	5.7667e-3	5.24812e-3	5.21005e-3

Table 1: Errors corresponding to different values of the ϵ for the three different cases of the test in Subsection 5.1.

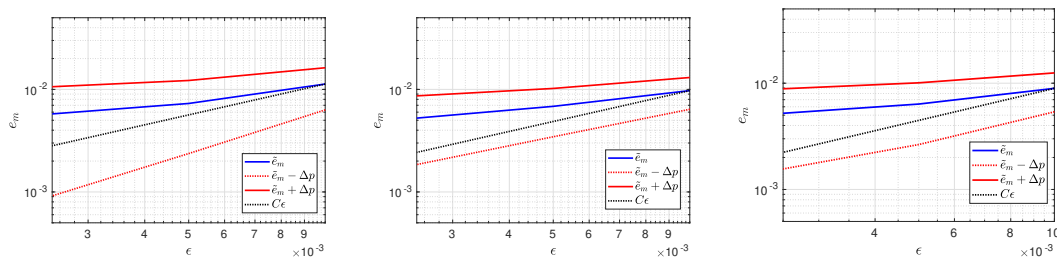


Figure 7: Estimate of the model error, upper and lower bounds compared with a linear trend in ϵ for case (i), case (ii) and case (iii) from left to right.

not well captured by the coarse mixed-dimensional grid.

For a more quantitative analysis we compute \tilde{e}_m as the $L^2(\Omega)$ norm of $I^\eta(p_\Omega^h) - p_{\text{equi}}^\eta$ for different apertures ϵ of the fault and surrounding layers. If the geometrical reduction is consistent we expect a reduction of this error with smaller values of ϵ . The results for the three cases are reported in Table 1. Note that as ϵ decreases we observe a saturation of the error. This is due to the fact that we are indeed measuring together the model error and the numerical error, i.e. the error due to a coarse mixed-dimensional grid.

To isolate the two effects we proceed as follows. Assuming that p_{equi}^η is fully resolved and can replace the exact equi-dimensional solution, we define the model error as

$$e_m = \|I^\eta(p_\Omega^{\text{exact}}) - p_{\text{equi}}^\eta\|_{L^2(\Omega)}$$

where p_Ω^{exact} is the fully resolved mixed-dimensional solution, which is in general not available since the aim of reduced model is to avoid extreme refinement. Let $p_\Omega^{h_2}$ be the solution for a second mixed-dimensional grid with $h_2 < h$, then

$$\begin{aligned} e_m &= \|I^\eta(p_\Omega^{\text{exact}}) - p_{\text{equi}}^\eta\|_{L^2(\Omega)} = \|I^\eta(p_\Omega^{\text{exact}}) + I^\eta(p_\Omega^h) - I^\eta(p_\Omega^h) - p_{\text{equi}}^\eta\|_{L^2(\Omega)} \\ &\leq \|I^\eta(p_\Omega^{\text{exact}}) - I^\eta(p_\Omega^h)\|_{L^2(\Omega)} + \|I^\eta(p_\Omega^h) - p_{\text{equi}}^\eta\|_{L^2(\Omega)} \\ &\leq \|I^\eta(p_\Omega^{\text{exact}}) - I^\eta(p_\Omega^{h_2})\|_{L^2(\Omega)} + \|I^\eta(p_\Omega^{h_2}) - I^\eta(p_\Omega^h)\|_{L^2(\Omega)} + \|I^\eta(p_\Omega^h) - p_{\text{equi}}^\eta\|_{L^2(\Omega)} \\ &= e_{h_2} + \Delta p + \tilde{e}_m \end{aligned}$$

Here \tilde{e}_m is the previous - incorrect - estimate of the model error, and Δp estimates the effect of grid refinement. If we assume that e_{h_2} is small, since $h_2 < h$, then we state that $e_m \leq \tilde{e}_m + \Delta p$. With similar arguments we can also obtain $e_m \geq \tilde{e}_m - \Delta p$. The values of this upper and lower bounds are reported for the three cases in Figure 7, where we can observe that the lower bound decreases linearly with ϵ as expected.

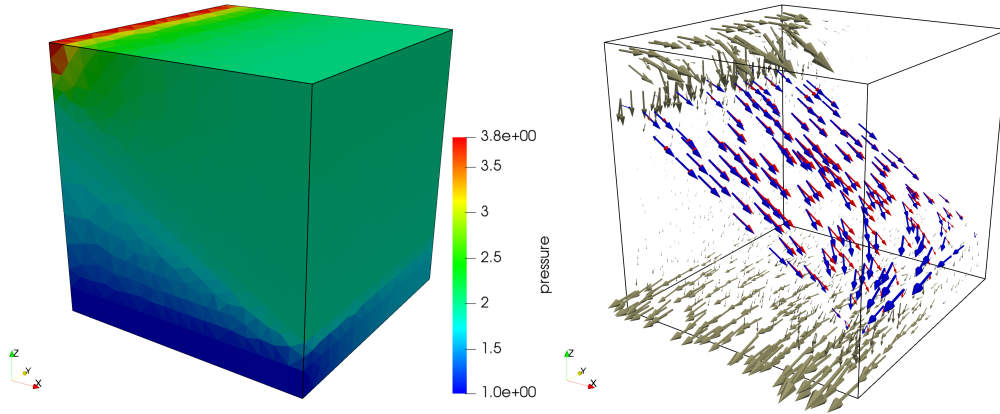


Figure 8: Graphical representation of the solution of the example in Subsection 5.2. On the left the pressure field, on the right the velocity field with different colours. With grey arrows we indicate the velocity in the rock matrix, with blue and red in the upper and lower part of the damage zone, respectively. The velocity in the fault is zero, then not represented.

5.2 A three-dimensional example

This last test case is inspired by *Case 1: single fracture* of the benchmark initiative [6]. We consider a single fault immersed in a three-dimensional rock matrix, defined as $\Omega = (0, 100)^3$. The fault has thickness equal to $\epsilon_\gamma = 10^{-3}$ and permeability equal to $\alpha_\gamma^2 = 10^{-7}\epsilon_\gamma$ and $\alpha_\Gamma^2 = 10^{-7}/\epsilon_\gamma$. The fault is identified by the following four corners

$$c_0 = (0, 0, 80) \quad c_1 = (100, 0, 20) \quad c_2 = (100, 100, 20) \quad c_3 = (0, 100, 80).$$

In the rock matrix the permeability is $\alpha_\Omega^2 = 10^{-6}$ for $z \geq 10$, otherwise $\alpha_\Omega^2 = 10^{-5}$. For the boundary condition, we impose 4 for the pressure in the narrow band $\{0\} \times (0, 100) \times (90, 100)$ and 0 in the portion $(0, 100) \times \{0\} \times (0, 100)$ of the boundary. We assume zero flux elsewhere. For the damage zone we have a thickness, greater than the fault, equal to $\epsilon_\mu = 10^{-1}$ with permeability $\alpha_\mu^2 = 10^{-2}\epsilon_\mu$ and $\alpha_M^2 = 10^{-2}/\epsilon_\mu$ on the upper part and $\alpha_\mu^2 = 10^{-1}\epsilon_\mu$ and $\alpha_M^2 = 10^{-1}/\epsilon_\mu$ on the lower part. The numerical solution considers a grid composed of $\sim 9.5k$ tetrahedra for Ω , 757 triangles for the fault grid γ , and $\sim 1.5k$ triangles for the damage zone μ . This corresponds to the coarsest mesh of the benchmark [6].

In Figure 8, we present the obtained numerical solution. On the left the pressure field; since the fault is less permeable than the damage zone and rock matrix the solution exhibits a steep variation across the fault. On the right the velocity is represented with different colours for the rock matrix, fault, and each part (top in blue and bottom in red) of the damage zone. The arrows corresponding to the rock matrix and the bottom part of the damage zone are enlarged by a factor 10^8 , while for the upper part of the damage zone we use a factor 10^9 . The velocity along the fault is zero because of its low permeability. Since the rock matrix is much less permeable than the damage zone the flow tends to be more concentrated in the latter. The arrows are coherently pointing from the inflow part to the outflow

Also in this three-dimensional case, the obtained solution is physically sound and shows the capability and potentiality of the model.

6 Conclusion

In this work we have introduced a new conceptual model for the simulation of Darcy flows in porous media crossed by large faults, i.e. by complex regions characterized by an inner thin core surrounded by damage zone where, due to the accommodation of strain, a large number of small fractures is present. Following a well established literature, we approximate the thin fault region, and in particular both the core and the damage zone as lower-dimensional and geometrically coincident objects, i.e. lines in $2d$ and surfaces in $3d$ to avoid extreme mesh refinement. However, unlike previous works, the presence of three lower dimensional interfaces instead of a single fault object gives us the freedom to better characterize the fluid-dynamic behavior of the structure, by using different permeability and a different thickness for the core and the damage zone, and even accounting for asymmetries across the fault. Moreover, we highlight the fact that this approach can be extended, in different areas of application, to the efficient simulation of thin layered porous media.

We have proven the well posedness of the weak formulation of the mixed dimensional problem and discussed its numerical approximation and a set of examples. The numerical tests confirm the ability of the resulting numerical scheme to handle high contrasts in permeability among the rock matrix, fault, and damage zone. Moreover, by comparing the mixed dimensional solution with fully resolved equi-dimensional simulations we have shown that the model error associated with geometrical model reduction is only focused where the fault or the damage zone give a jump in the pressure field and, moreover, this error decreases for thinner faults as expected. The obtained solutions are thus physically sound and the model can be regarded as a promising strategy. Possible future developments include the possibility to account for heterogeneities, and changes in time, in the aperture and permeability of the different layers. These variability could be the result of geochemical or mechanical processes. Moreover we plan to couple the flow problem with transport, to fully exploit the freedom and flexibility given by the detailed description of the permeability of the layers. We remark that the coupling with transport which is natural thanks to the mixed conservative approximation of the velocity field.

7 Acknowledgements

We acknowledge the PorePy development team: Runar Berge, Inga Berre, Eirik Keilegavlen, and Ivar Stefansson. Finally, the authors warmly thanks Stefano Scialò for many fruitful discussions.

References

- [1] Raheel Ahmed, Micheal G. Edwards, Sadok Lamine, Bastiaan A. H. Huisman, and Mayur Pal. Control-volume distributed multi-point flux approximation coupled with a lower-dimensional fracture model. *Journal of Computational Physics*, 284:462–489, 2015.
- [2] Clarisse Alboin, Jérôme Jaffré, Jean E. Roberts, Xuwen Wang, and Christophe Serres. Domain Decomposition for some Transmission Problems in Flow in Porous Media. In *Numerical treatment of multiphase flows in porous media (Beijing, 1999)*, volume 552 of *Lecture Notes in Phys.*, pages 22–34. Springer, Berlin, 2000.
- [3] Philippe Angot, Franck Boyer, and Florence Hubert. Asymptotic and numerical modelling of flows in fractured porous media. *M2AN Math. Model. Numer. Anal.*, 43(2):239–275, 2009.

- [4] Paola Francesca Antonietti, Luca Formaggia, Anna Scotti, Marco Verani, and Nicola Verzotti. Mimetic finite difference approximation of flows in fractured porous media. *ESAIM: M2AN*, 50(3):809–832, 2016.
- [5] Jacob Bear, Chin-Fu Tsang, and G de Marsily. *Flow and contaminant transport in fractured rock*. Academic Press, San Diego, 1993.
- [6] Inga Berre, Wietse Boon, Bernd Flemisch, Alessio Fumagalli, Dennis Gläser, Eirik Keilgavlen, Anna Scotti, Ivar Stefansson, and Alexandru Tatomir. Call for participation: Verification benchmarks for single-phase flow in three-dimensional fractured porous media. Technical report, arXiv:1809.06926 [math.NA], 2018.
- [7] Wietse M. Boon, Jan M. Nordbotten, and Ivan Yotov. Robust discretization of flow in fractured porous media. *SIAM Journal on Numerical Analysis*, 56(4):2203–2233, 2018.
- [8] Konstantin Brenner, Julian Hennicker, Roland Masson, and Pierre Samier. Gradient discretization of hybrid-dimensional Darcy flow in fractured porous media with discontinuous pressures at matrix–fracture interfaces. *IMA Journal of Numerical Analysis*, September 2016.
- [9] Konstantin Brenner, Julian Hennicker, Roland Masson, and Pierre Samier. Hybrid-dimensional modelling of two-phase flow through fractured porous media with enhanced matrix fracture transmission conditions. *Journal of Computational Physics*, 357:100–124, 2018.
- [10] Kostantin Brenner, Mayya Groza, C. Guichard, and Roland Masson. Vertex approximate gradient scheme for hybrid dimensional two-phase darcy flows in fractured porous media. *ESAIM: Mathematical Modelling and Numerical Analysis*, 49(2):303–330, 2015.
- [11] Franco Brezzi and Michel Fortin. *Mixed and Hybrid Finite Element Methods*, volume 15 of *Computational Mathematics*. Springer Verlag, Berlin, 1991.
- [12] Carlo D’Angelo and Anna Scotti. A mixed finite element method for Darcy flow in fractured porous media with non-matching grids. *Mathematical Modelling and Numerical Analysis*, 46(02):465–489, 2012.
- [13] Marco Del Pra, Alessio Fumagalli, and Anna Scotti. Well posedness of fully coupled fracture/bulk darcy flow with xfem. *SIAM Journal on Numerical Analysis*, 55(2):785–811, 2017.
- [14] Gerhard Dziuk. Finite Elements for the Beltrami operator on arbitrary surfaces. In Stefan Hildebrandt and Rolf Leis, editors, *Partial Differential Equations and Calculus of Variations*, volume 1357 of *Lecture Notes in Mathematics*, pages 142–155. Springer Berlin Heidelberg, 1988.
- [15] Isabelle Faille, Eric Flauraud, Frédéric Nataf, Sylvie Pégaz-Fiornet, Frédéric Schneider, and Françoise Willien. A New Fault Model in Geological Basin Modelling. Application of Finite Volume Scheme and Domain Decomposition Methods. In *Finite volumes for complex applications, III (Porquerolles, 2002)*, pages 529–536. Hermes Sci. Publ., Paris, 2002.
- [16] Isabelle Faille, Alessio Fumagalli, Jérôme Jaffré, and Jean Elisabeth Roberts. Model reduction and discretization using hybrid finite volumes of flow in porous media containing faults. *Computational Geosciences*, 20(2):317–339, 2016.

- [17] Bernd Flemisch, Inga Berre, Wietse Boon, Alessio Fumagalli, Nicolas Schwenck, Anna Scotti, Ivar Stefansson, and Alexandru Tatomir. Benchmarks for single-phase flow in fractured porous media. *Advances in Water Resources*, 111:239–258, Januray 2018.
- [18] Luca Formaggia, Alessio Fumagalli, Anna Scotti, and Paolo Ruffo. A reduced model for Darcy’s problem in networks of fractures. *ESAIM: Mathematical Modelling and Numerical Analysis*, 48:1089–1116, 7 2014.
- [19] Najla Frih, Vincent Martin, Jean Elisabeth Roberts, and Ai Saâda. Modeling fractures as interfaces with nonmatching grids. *Computational Geosciences*, 16(4):1043–1060, 2012.
- [20] Alessio Fumagalli and Isabelle Faille. A double-layer reduced model for fault flow on slipping domains with hybrid finite volume scheme. *SIAM Journal on Scientific Computing*, pages 1–26, June 2018.
- [21] Alessio Fumagalli and Eirik Keilegavlen. Dual virtual element method for discrete fractures networks. *SIAM Journal on Scientific Computing*, 40(1):B228–B258, 2018.
- [22] Alessio Fumagalli and Anna Scotti. A numerical method for two-phase flow in fractured porous media with non-matching grids. *Advances in Water Resources*, 62, Part C(0):454–464, 2013. Computational Methods in Geologic CO2 Sequestration.
- [23] Hussein Hoteit and Abbas Firoozabadi. An efficient numerical model for incompressible two-phase flow in fractured media. *Advances in Water Resources*, 31(6):891–905, June 2008.
- [24] Mun-Hong Hui, Bradley T. Mallison, and Kok-Thye Lim. An innovative workflow to model fractures in a giant carbonate reservoir. In *International Petroleum Technology Conference, 3-5 December, Kuala Lumpur, Malaysia, 2008*.
- [25] Jérôme Jaffré, Vincent Martin, and Jean E. Roberts. Generalized cell-centered finite volume methods for flow in porous media with faults. In *Finite volumes for complex applications, III (Porquerolles, 2002)*, pages 343–350. Hermes Sci. Publ., Paris, 2002.
- [26] Jérôme Jaffré, Mokhles Mnejja, and Jean E. Roberts. A discrete fracture model for two-phase flow with matrix-fracture interaction. *Procedia Computer Science*, 4:967–973, 2011.
- [27] Mohammad Karimi-Fard and Luis J. Durlofsky. A general gridding, discretization, and coarsening methodology for modeling flow in porous formations with discrete geological features. *Advances in Water Resources*, 96:354–372, oct 2016.
- [28] Mohammad Karimi-Fard, Bin Gong, and Luis J. Durlofsky. Generation of coarse-scale continuum flow models from detailed fracture characterizations. *Water Resources Research*, 42(10), 2006.
- [29] Eirik Keilegavlen, Alessio Fumagalli, Runar Berge, Ivar Stefansson, and Inga Berre. Porepy: An open source simulation tool for flow and transport in deformable fractured rocks. Technical report, arXiv:1712.00460 [cs.CE], 2017.
- [30] Peter Knabner and Jean Elisabeth Roberts. Mathematical analysis of a discrete fracture model coupling darcy flow in the matrix with darcy-forchheimer flow in the fracture. *ESAIM: Mathematical Modelling and Numerical Analysis*, 48:1451–1472, 9 2014.
- [31] Vincent Martin, Jérôme Jaffré, and Jean Elisabeth Roberts. Modeling Fractures and Barriers as Interfaces for Flow in Porous Media. *SIAM J. Sci. Comput.*, 26(5):1667–1691, 2005.

- [32] Fernando Morales and Ralph E. Showalter. The narrow fracture approximation by channelled flow. *Journal of Mathematical Analysis and Applications*, 365(1):320–331, 2010.
- [33] Fernando Morales and Ralph E. Showalter. Interface approximation of darcy flow in a narrow channel. *Mathematical Methods in the Applied Sciences*, 35(2):182–195, 2012.
- [34] Jan Martin Nordbotten, Wietse Boon, Alessio Fumagalli, and Eirik Keilegavlen. Unified approach to discretization of flow in fractured porous media. *Computational Geosciences*, 2018.
- [35] Volker Reichenberger, Hartmut Jakobs, Peter Bastian, and Rainer Helmig. A mixed-dimensional finite volume method for two-phase flow in fractured porous media. *Advances in Water Resources*, 29(7):1020–1036, 2006.
- [36] Jean E. Roberts and Jean-Marie Thomas. Mixed and hybrid methods. In *Handbook of numerical analysis, Vol. II*, Handb. Numer. Anal., II, pages 523–639. North-Holland, Amsterdam, 1991.
- [37] Tor Harald Sandve, Inga Berre, and Jan Martin Nordbotten. An efficient multi-point flux approximation method for Discrete Fracture-Matrix simulations. *Journal of Computational Physics*, 231(9):3784–3800, 2012.
- [38] Nicolas Schwenck, Bernd Flemisch, Rainer Helmig, and BarbaraI. Wohlmuth. Dimensionally reduced flow models in fractured porous media: crossings and boundaries. *Computational Geosciences*, 19(6):1219–1230, 2015.
- [39] Anna Scotti, Luca Formaggia, and Federica Sottocasa. Analysis of a mimetic finite difference approximation of flows in fractured porous media. *ESAIM: M2AN*, 2017.
- [40] Xavier Tunc, Isabelle Faille, Thierry Gallouët, Marie Christine Cacas, and Pascal Havé. A model for conductive faults with non-matching grids. *Computational Geosciences*, 16:277–296, 2012.